Eindhoven University of Technology

MASTER

Relation between structure and properties in PLA

Sterrenburg, M.

Award date:
2011

Link to publication

Disclaimer
This document contains a student thesis (bachelor's or master's), as authored by a student at Eindhoven University of Technology. Student theses are made available in the TU/e repository upon obtaining the required degree. The grade received is not published on the document as presented in the repository. The required complexity or quality of research of student theses may vary by program, and the required minimum study period may vary in duration.

General rights
Copyright and moral rights for the publications made accessible in the public portal are retained by the authors and/or other copyright owners and it is a condition of accessing publications that users recognise and abide by the legal requirements associated with these rights.

- Users may download and print one copy of any publication from the public portal for the purpose of private study or research.
- You may not further distribute the material or use it for any profit-making activity or commercial gain

m sterrenburg
augustus 2011

Masterthesis

Relation between structure and properties in PLA

M. Sterrenburg

Supervisors:

Prof. Dr. Ir. H.E.H. Meijer

Dr. Ir. L.E. Govaert

Dr.Ir. L. Balzano

Eindhoven University of Technology

Department of Mechanical Engineering

Materials Technology

Eindhoven, August 19, 2011

Contents

Abstract

Poly(L-lactic acid), PLLA, is a polymer based on the renewable lactic acid monomer. The big advantage for medical devices is that PLLA can be biocompatible and bioresorable. In this way, the material can be used for orthopaedic fixation that, after the patient has recovered, does not need to be removed as theyare, instead, metabolized by the body. However, the mechanical performance of PLLA has two major drawbacks: brittle failure and poor durability.

The poor durability of the PLLA is a consequence of stress-enhanced molecular motion. This phenomenon can be restricted by engaging molecules within crystals. Therefore, to enhance durability, PLLA is crystallized in this study. This is done with two routes: annealing above T_g and blending with poly(D-lactic acid) to form stereo complexes. Creep experiments shows that the durability has improved. Blends with core-shell nano particles are tested to investigate the change in toughness.

1 Introduction

Poly-Lactic acid, PLA, is a polymer based on the renewable lactic acid monomer. Lactic acid can be produced on industrial scale by bacteria and then converted in the polymer with different processes. The market for PLA products includes mechanical devices and is continuously growing because of the advantageous properties of this material, e.g. degradability and high yield stress.

PLA has two enantiomers: poly(L-lactic acid) (PLLA) and poly(D-lactic acid) (PDLA). PLLA is the focus of this study.

The big advantage for medical devices is that PLLA can be biocompatible and bioresorable. In this way, the material can be used for orthopaedic fixation that, after the patient has recovered, does not need to be removed as theyare, instead, metabolized by the body. Because of the high modulus and yield strength (short-term mechanical properties), PLLA is a potential candidate to make load-bearing devices including cages for spinal surgery.

However, the mechanical performance of PLLA has two major drawbacks:

- it is susceptible to brittle fracture
- it displays a poor resistance to continuous loading

A previous study on in-vivo PLLA spinal cages in a goat model showed that the implants failed prematurely [1]. This suggests that, despite the excellent short-term mechanical properties, the long term mechanical response (durability) is rather poor.

The aim of this study is to enhance the mechanical properties of PLLA by making it:

- more durable
- less brittle

The poor durability of the PLLA is a consequence of stress-enhanced molecular motion. This phenomenon can be restricted by engaging molecules within crystals. Therefore, to enhance durability, we aim to make PLLA crystallize. This can be done with two routes:

- annealing above T_g
- blending with PDLA to form stereo complexes

Nevertheless, crystallization is not expected to make the material tougher. To tackle this issue we use a different strategy: the addition of core-shell nano-particles.

For the sake of clarity, results in this manuscript are divided in 3 parts:

- Part I: Effect of crystallinity on mechanics of PLLA
- Part II: Enhancing crystallization of PLLA
- Part III: Toughness of PLLA

2 Materials and methods

2.1 Materials

The material used in part I of this study is poly(L-lactic acid), IV 4.2 dl/g, provided by Purac Biochem (Gorinchem, The Netherlands).

The material in part II and III is poly(L-lactic acid), IV 3.8 dl/g, also provided by Purac Biochem.

The relation between intrinsic viscosity (IV) and the average molecular weight (M_w in [kDa]) is described by the Mark-Houwink relation:

$$M_w = \left(\frac{IV}{K}\right)^{\frac{1}{\alpha}}$$

For PLLA $K = 5.45 \cdot 10^{-4}$ and α=0.73. [2]

Poly(D-lactic acid), IV 0.9dl/g and poly(D-lactic acid),IV 0.4 dl/g are blended with poly(L-lactic acid) to enhance the crystallinity. These materials are also provided by Purac Biochem.

In this work, the materials are, according to high and low molecular weight, labelled respectively as PDLA_HMw and PDLA_LMw,

Paraloid EXL 2330 (Rohm & Haas) is used in part III as a toughening agent and will further be referred to as EXL. It consists of poly(butylacrylate)-poly(methyl methacrylate) core-shell particles of approximately 110 nm in diameter.

2.2 Sample preparation

2.2.1 Samples for part I

For compression tests, granules were first dried for 2 days in a vacuum oven, then compression moulded into 10 mm thick rectangular plaques at 200°C and, eventually, rapidly cooled to room temperature. Bars with a thickness of 10 mm were sawed from the compression moulded plaques. After annealing them for 7 hours at 80°C, cylinders with a diameter and height of 6 mm were machined.

2.2.2 Samples for part II and III

For compression tests, granules were first dried for 2 days in a vacuum oven, then compression moulded into 5 mm thick rectangular bars at respectively 210°C for pure PLLA and 240°C for the blends.

Eventually, the bars were rapidly cooled to room temperature by water cooled plates. At the end, cylindrical specimens with a diameter and height of 4 mm were machined from the bars.

For tensile tests, the granules were compression moulded into 1 mm thick plaques at 210°C for pure PLLA and 240°C for the blends. After moulding, the plaques were rapidly cooled to room temperature. Eventually tensile bars with gauge sections of 35x4.5x1mm^3 were machined out of these plaques.

The blends with PDLA are labelled PLLA_PDLA_XMw_y/z where X (= H for high molecular weight and L for low molecular weight), y and z the mass percentage of the parent polymer and of the PDLA, respectively.
For every blend, in total 3 grams of material were dissolved in dichloromethane at room temperature, according to Tsuji et al. [3]. To enhance the dissolution rate, mechanical shaking was applied until the suspension became transparent, typically after 4 hours. Afterwards, the solute was precipitated into stirred ethanol (8 times in excess) and isolated through vacuum filtration. To remove the left-over solvent, the precipitates were dried for 24 h under vacuum at room temperature.

Samples for mechanical testing require larger amounts of material and so large amounts of solvents, which is not desirable. Hence, for mechanical testing material is blended by extrusion at 240°C, after drying for 2 days in vacuum at room temperature.

In part III PLLA and PLLA_PDLA_LMw_60/40 are blended by extrusion at 240°C, with a mass percentage of 15 EXL, labelled as respectively PLLA+15EXL and PLLA_PDLA_LMw_60/40+15EXL.

2.3 Methods

Uniaxial compression tests were performed on a servo-hydraulic MTS Elastomer Testing System 810 and 831 equiped with a temperature chamber and on a Zwick Z010 universal tester. Friction between the samples and compression plates was reduced by applying a thin film of skived PTFE tape (3M 5480) on the sample end and spraying PTFE lubricant on the compression plates. Constant strain rate experiments were performed in true strain control at rates varying from 10^{-2} to 10^{-5} s^{-1}. Creep experiments were performed in true stress control at various stress levels. All loads were calculated under the assumption of incompressibility.

Tensile tests were performed on a Zwick Z010 and a Zwick 1475 universal tensile tester equipped with a temperature chamber. Constant strain rate experiments were performed in true strain control at rates varying from 10^{-2} to 10^{-5} s^{-1}. Creep experiments were performed in true stress control at various stress levels.

Tensile tests in water were performed on a servo-hydraulic MTS Elastomer Testing System 810 equipment and on a Zwick Z010 universal tensile tester. Water was heated at 37°C and pumped by a Lauda MS/2 equipment. The schematic set-up is shown in Figure 2.1

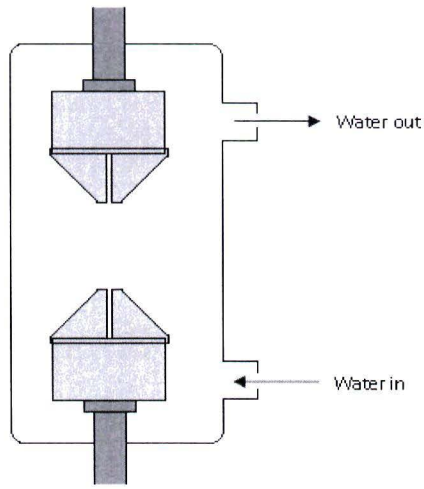

Figure 2.1 Set-up for tensile testing in water

Differential scanning calorimetry (DSC) was performed on a Mettler Toledo DSC823e equipped with a FRS5 sensor.

WAXD was performed at the beamline BM26 of the E.S.R.F. . Samples were irradiated with a wavelength of 1.24 Å. The diffraction pattern was recorded on a Dectris Pilatus 300K with a pixel size of 44 x 44µm placed at about 150 mm from the sample.

3 Background

3.1 Phenomenology and ductile failure

The short term mechanical properties can be examined with uniaxial compression tests. Here, benefitting from homogeneous deformation, the intrinsic stress-strain response of the material is measured. An example is provided in Figure 3.1a.

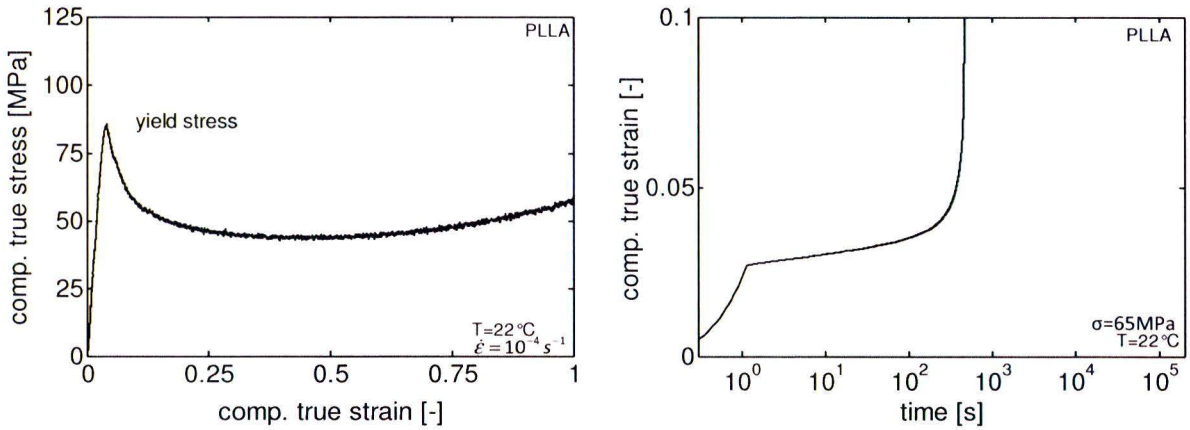

Figure 3.1(a) Compression test at constant strain rate (b) Creep test under constant load

At small strain, in the elastic regime, stress increases linearly with deformation. At larger strain, the response becomes non-linear and stress reaches a maximum, the *yield stress* (σ_y).

Yielding marks the onset of plastic deformation. From there onwards, the response shows two phenomena: (1) *strain softening,* the initial decrease of true stress with strain and (2) *strain hardening*, the subsequent upswing of the true stress-strain curve.

These two post-yield phenomena play an important role in the mode of failure. Materials with weak softening and strong hardening behave ductile; materials with strong softening and weak hardening (like PLLA) behave brittle.

The long-term performance of PLLA is shown in Figure 3.1b, where a creep experiment shows the deformation of a specimen under constant compressive load. Despite the temperature is below T_g, even when loaded at $\sigma<\sigma_y$ after some time, the material exhibits a fluid-like behaviour.

The response of the material depends strongly on loading conditions, as illustrated in Figure 3.2.

For a constant applied strain rate, the overall stresses increases with strain rate, see Figure 3.2a . While during a creep test, time-to-failure decreases with stress, see Figure 3.2b.

The rate dependence of the yield stress and stress-dependence of the time-to-failure of PLLA are shown in Figure 3.3. Remarkably, in both cases, a semi-logarithmic relation is observed with a slope α for the strain rate dependence of the yield stress and a slope −α for the time-to-failure dependence of the stress. This suggests that these two phenomena are strongly related. Moreover, Figure 3.3 illustrates that, under a static load a material will, sooner or later, fail.

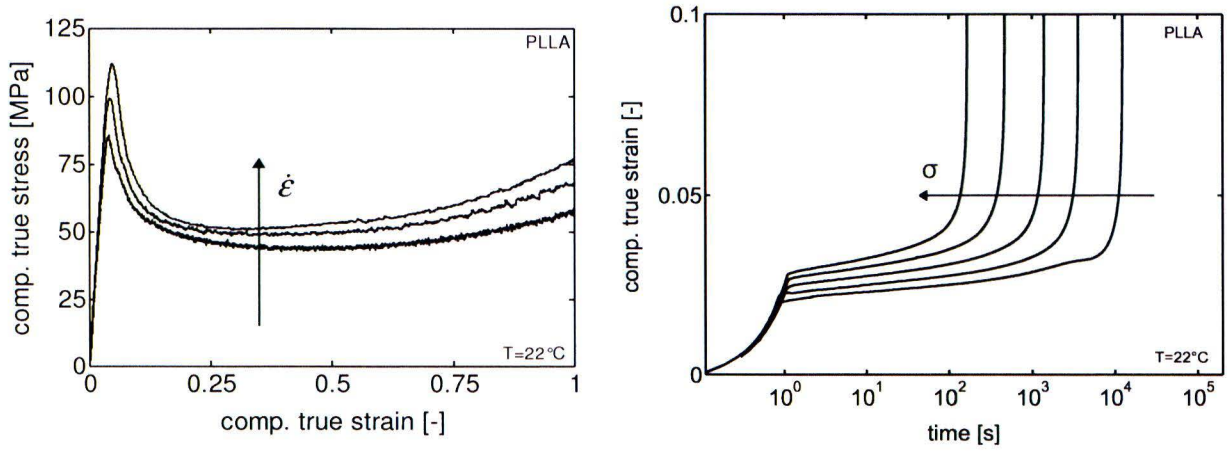

Figure 3.2 (a) Compression curves for several strain rates (b) True strain vs. loading time for increasing stresses

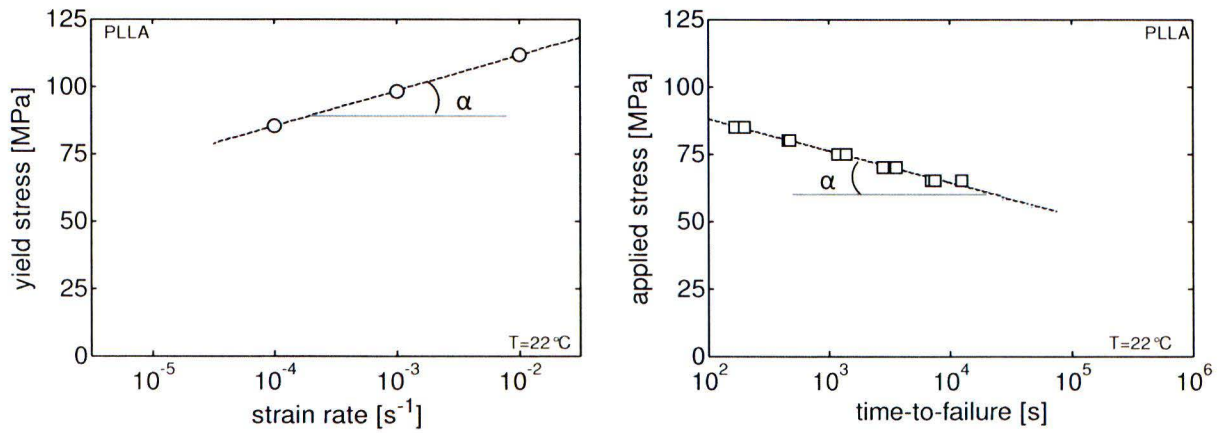

Figure 3.3 (a) Rate dependence of yield stress (b) Stress dependence of the time-to-failure

The slope α is important for studying durability. The yield stress of PLLA increases 14 MPa per decade of strain rate, much more than other polymers such as polycarbonate (PC) where it increases only about 3 MPa per decade, see Figure 3.4.

This means that to decrease the time-to-failure one order of magnitude for PC the applied stress has to be decreased with 3 MPa, whereas for PLLA this has to be 14 MPa. For PLLA this results in a very poor durability, illustrated in Figure 3.4b.

[4]

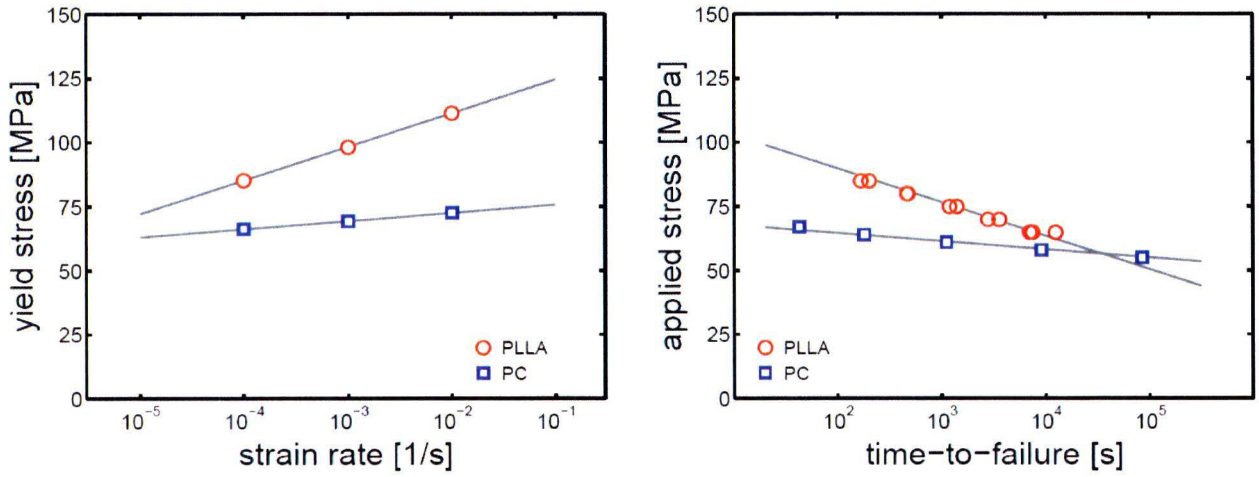

Figure 3.4 Uniaxial compression results for PLLA and PC. (a) Yield stress versus strain rate. (b) Applied stress versus time-to-failure

3.2 Molecular origin

The origin of the strain rate dependence of the yield stress (deformation kinetics) can be related to the molecular nature of the polymer.

Amorphous polymers consist of long, covalently-bonded molecules that are randomly arranged in the material. Depending on stress and temperature, molecules have the ability to change spatial conformation by main-chain segmental motions.

At high temperatures, above T_g, chains can move freely with applied deformations (rubber-like behaviour). At low temperature, below T_g, the mobility decreases drastically and the material becomes a glass. Changes in spatial conformations are still possible, although only over long timescales.

When stress is applied, the scenario can drastically change. Similar to temperature, stress induces a state of enhanced molecular mobility, leading to mobility similar to the melt-state. The deformation behaviour can therefore be seen as a sort of fluid-like behaviour with very high viscosity.

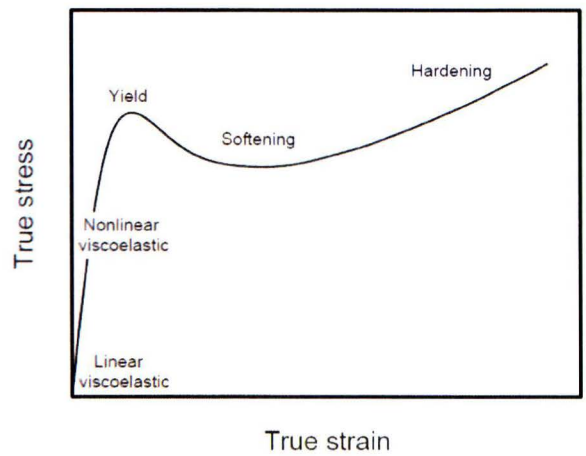

Figure 3.5 Schematic representation of the intrinsic deformation behaviour of a polymer material

To illustrate this, the yield point is investigated closer and a schematic representation of intrinsic deformation behaviour is given in Figure 3.5. In the initial state of loading, at the start of the test, the applied strain rate causes a low stress and chain mobility is negligible. The modulus at this point is determined by the intermolecular interactions between individual chains.

At increasing strain, the stress increases and also the chain mobility increases. Changes in chain conformation gradually start to contribute to the deformation of the material. This contribution strongly increases, until the stress level is reached where the plastic strain rate matches the applied strain rate. This flow contribution defines the yield point. In other words, the applied stress at yield induces a state of mobility resulting in a steady state of plastic flow, $\dot{\varepsilon}_{pl}$.

The magnitude of this plastic flow depends on the applied stress and temperature. At higher strain rates, a higher stress is needed to induce a higher mobility. As a result, the yield stress is observed to increase with strain rate.

A steady rate of plastic flow can also be observed in static load experiments, as illustrated Figure 3.2b. The evolution of strain rate during creep can be visualized by plotting the strain rate as a function of strain, the so-called Sherby-Dorn plot [5], see Figure 3.6a.

In this plot, three regions are observed: the first region is characterized by a decreasing strain rate (primary creep), the second by a steady strain rate (secondary creep) and the last by an increasing strain rate (tertiary creep).

The constant strain rate ($\dot{\varepsilon}_{min}$) during secondary creep indicates the steady rate of plastic flow.

Bauwens-Crowet et al. [6] were the first to demonstrate that the flow at the yield point in a constant applied strain rate experiment is identically to the flow during secondary creep in static load experiments, demonstrated in Figure 3.6b.

Summarizing: in polymer glasses stress enhances molecular mobility , triggering a steady rate of plastic flow.[4]

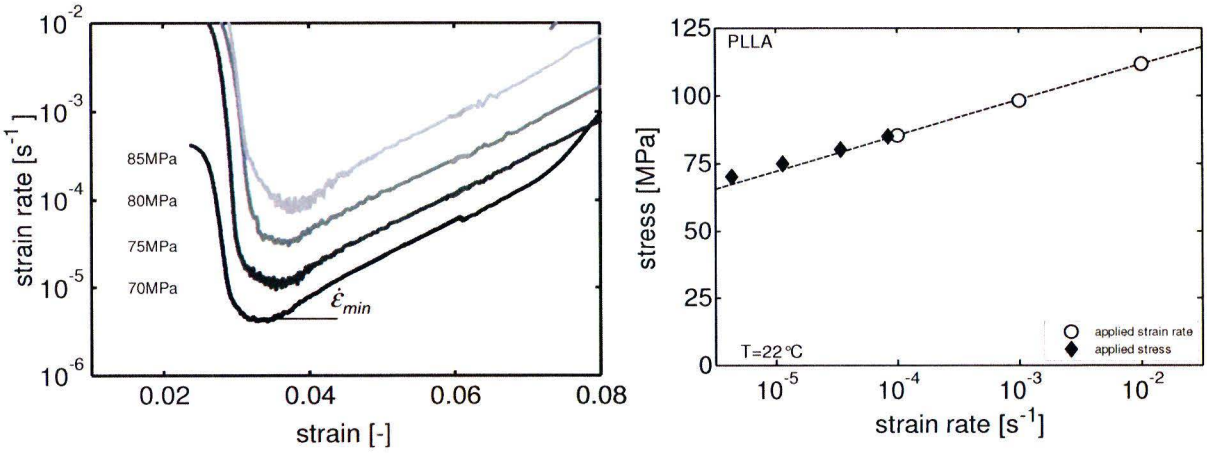

Figure 3.6 (a) Sherby-Dorn plot for several applied stresses; (b) Strain rates from applied stress and applied strain rate

Under a constant stress, the material cannot flow indefinitely. At a certain point, softening takes place and tremendously accelerates deformation leading to strain localization, i.e. failure. This occurs always at the same plastic strain, the critical strain ε_{cr}. In other words, failure takes place when $\varepsilon_{pl} \geq \varepsilon_{cr}$.

The use of ε_{cr} enables the quantitative prediction of time-to-failure using the stress dependence of plastic flow.

The time-to-failure can be determined by:

$$t_f(\sigma,T) = \frac{\varepsilon_{cr}}{\dot{\varepsilon}_{pl}(\sigma,T)} \tag{1}$$

3.3 Deformation kinetics

The ability of polymers to deform is determined by the mobility of its molecules. This is characterized by specific molecular motions and relaxation mechanisms. A distinction can be made between materials with a single relaxation mechanism (thermorheological simple materials) and materials with multiple relaxation mechanisms (thermorheological complex materials).

3.3.1 Thermorheological simple materials

The deformation of thermorheoligical simple materials is caused by a single relaxation process, referred as the α-process.

Polycarbonate (PC), is a well-known material and a good model to explain characteristics of thermorheological simple materials.

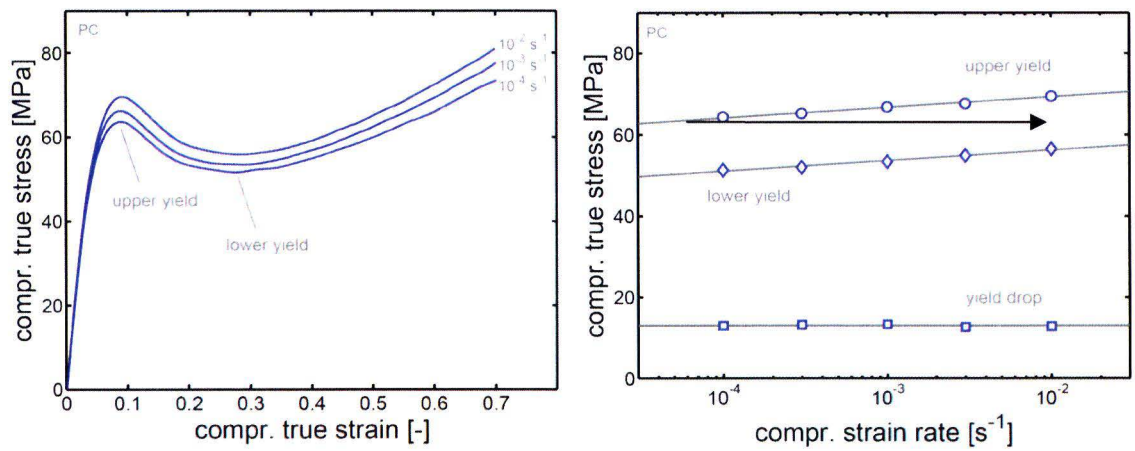

Figure 3.7 PC: (a) Compression curves; (b) Strain rate dependence of upper yield, lower yield and yield drop

The influence of strain rate on the intrinsic behaviour of PC is shown in Figure 3.7a. With an increasing strain rate, the yield stress increases.

Figure 3.7b illustrates the semi-logarithmic relation between strain rate and yield stress. The slope of this relation is constant over the whole range of strain rates.

The slope of the strain rate dependence of the lower yield (minimum of post-yield region) is identical to that of (upper) yield stress, resulting in a constant yield drop (difference between upper and lower yield). Further on, it is shown that the rate dependence of the lower yield can be determined by shifting the rate dependence of the yield stress to higher strain rate, as indicated by the arrow.[7]

The fluid-like behaviour of thermorheological simple materials under stress, with its strong strain-rate and temperature dependence can be described via Eyring's activated flow theory [8]:

$$\dot{\varepsilon}_{pl}(\sigma,T) = \underbrace{\dot{\varepsilon}_0}_{I} \cdot \underbrace{\exp\left(-\frac{\Delta U}{R \cdot T}\right)}_{II} \cdot \underbrace{\sinh\left(\frac{\sigma \cdot V^*}{k \cdot T}\right)}_{III} \tag{2}$$

Part I of equation (2) is the reference strain rate [s^{-1}] at an arbitrary temperature depending on the thermal history. Part II covers the temperature dependent deformation kinetics, where ΔU is the activation energy [J/mol], R the universal gas constant [J/(mol K)] and T the absolute temperature [K]. Part III covers the stress dependent deformation kinetics, with σ the stress [Pa], V^* the activation volume [m^3] and k the Boltzmann's constant [J/K].

At the yield point, the plastic strain rate is equal to the applied strain rate. Therefore, the strain rate dependence of the yield stress can be described by inverting equation (2):

$$\sigma_y(\dot{\varepsilon},T) = \frac{k \cdot T}{V^*} \cdot \sinh^{-1}\left(\frac{\dot{\varepsilon}}{\dot{\varepsilon}_0} \cdot \exp\left(\frac{\Delta U}{RT}\right)\right) \tag{3}$$

Where $\dot{\varepsilon}$ is the applied strain rate.

3.3.2 Thermorheological complex materials

The description of thermorheological simple materials is not suitable for all polymers.

Thermorheological complex materials have multiple relaxation mechanisms actively contributing to the deformation. To illustrate this, the behaviour of polymethylmethacrylate (PMMA) is illustrated in Figure 3.8.

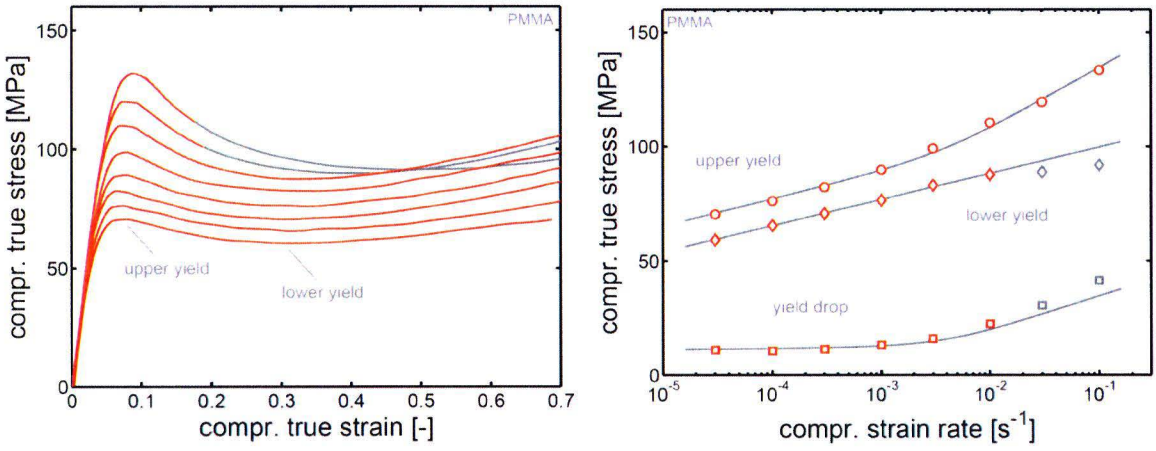

Figure 3.8 PMMA: (a) Compression curves; (b) Strain rate dependence of upper yield, lower yield and yield drop

As seen for PC, the yield stress increases with strain rate. But, in this case, the slope of the strain rate dependence of the yield stress changes, see Figure 3.8b.

At low strain rates, the upper and lower yield stress increase with the same slope, but at a certain strain rate, the upper yield shows an upswing due to a secondary relaxation mechanism, the β-process.

A schematic representation is given in Figure 3.9a. At low strain rate, only the α-process is contributing to deformation, at higher strain rate the β-process starts contributing.

Because of the β-relaxation mechanism, the single mode Eyring equation (3) is not sufficient to describe the behaviour of thermorheological complex materials.

A more accurate way to model this behaviour is the use of the Ree-Eyring modification [9] of Eyring's flow theory.

This modification, based on the assumption that two molecular processes (α and β) act in parallel, implies that the resulting stress is the sum of both processes.

The rate dependence of the system can be described as the sum of two individual Eyring processes:

$$\sigma(\dot{\varepsilon},T)=\sigma_\alpha+\sigma_\beta=\frac{kT}{V_\alpha^*}\sinh^{-1}\left(\frac{\dot{\varepsilon}}{\dot{\varepsilon}_{0,\alpha}}\exp\left(\frac{\Delta U_\alpha}{RT}\right)\right)+\frac{kT}{V_\beta^*}\sinh^{-1}\left(\frac{\dot{\varepsilon}}{\dot{\varepsilon}_{0,\beta}}\exp\left(\frac{\Delta U_\beta}{RT}\right)\right) \quad (4)$$

The lower yield can still be determined by shifting the upper yield to higher strain rates and the transition in kinetics is also expected to shift, resulting in three different regions, as illustrated in Figure 3.9b.

According to this representation, in region I and III the material exhibits a strain rate independent yield drop while in region II the material exhibits a strain rate dependent yield drop.[7]

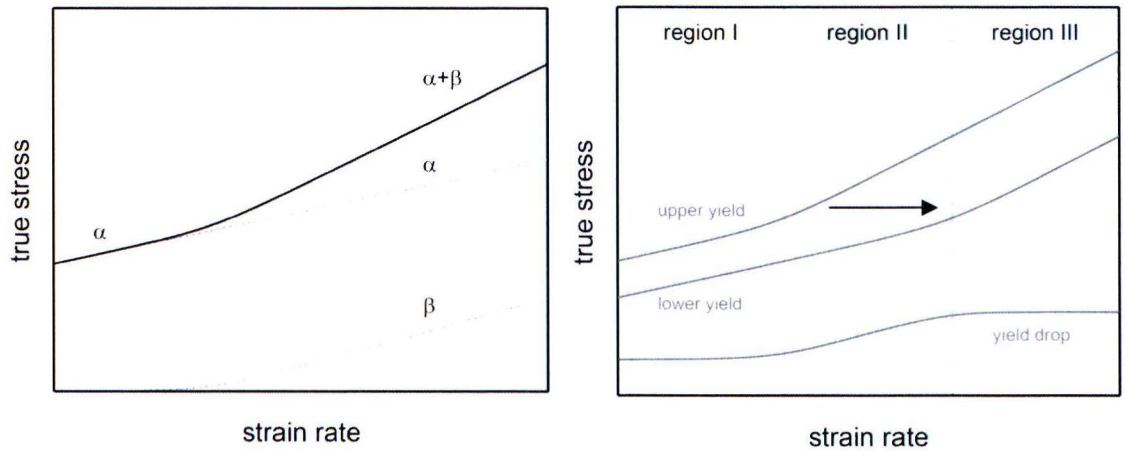

Figure 3.9 (a) Yield stress vs. strain rate for multiple relaxation mechanisms [10];
(b) Division of strain rate dependence into regions

Results

4 Part I: Effect of crystallinity on mechanics of PLLA

4.1 Crystallization of PLLA

Similar to other polyesthers, PLLA crystallizes slowly. The crystallization behaviour of PLLA is investigated by isothermal DSC experiments. Samples are heated to 240°C, kept at that temperature for two minutes in order to erase preivious histories, and subsequently cooled with a rate of 10°C/min to the isothermal crystallization temperature where they are held for long time.

In these experiments, crystallization is revealed by an exothermic peak in the heat flow, see Figure 4.1. The time to reach the peak maximum (crystallization time) changes with temperature.

When the crystallization temperature is represented as a function of the crystallization time, a time temperature transformation (TTT) plot is obtained (see Figure 4.1b).

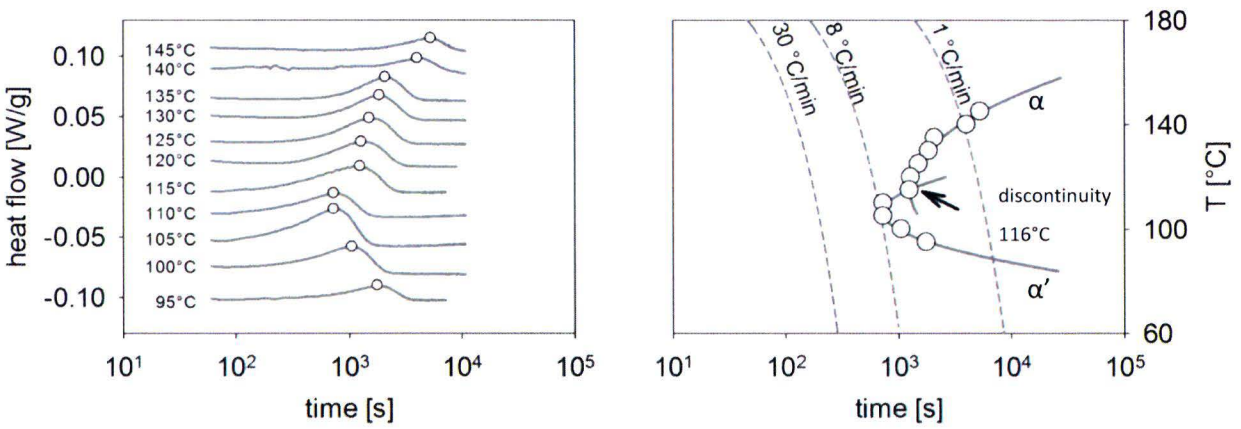

Figure 4.1(a) Change of time-to-peak (b) TTT-plot

The TTT-plot provides information to estimate the effect of different cooling rates on crystallization.

For an arbitrary thermal history T(t), the intersection with the TTT-line provides the crystallization time and temperature. At high cooling rates, T(t) does not intercept the TTT-line, suggesting that the material is quenched amorphous.

The critical cooling rate that defines the conditions leading to amorphous PLLA is:

$$\dot{T}_{cr} = \frac{T_m^0 - T_{mint}}{\Delta t} = \frac{203 - 105°C}{710s} = 0.138°C/s \approx 8°C/min$$

where T_m^0 is the equilibrium melting point of 203°C [11]; T_{mint} the temperature at the minimum time and Δt the minimum time.

The TTT provides also information on structure formation. For instance, the kink indicated by the arrow at 116°C represents a discontinuity in the crystallization rate of the material.

At crystallization temperatures above 116°C, PLLA crystallizes in the α-form. Below 116°C, it crystallizes as α'-form (disordered α-form), according to observations of Kawai et al. [12].

The α-form is orthorhombic with a=10.7, b=6.45 and c=28.8 Å, while the α'-form is hexagonal with a=b=6.2 and c=28.8 Å [12].

The existence of two types of crystals is confirmed by WAXD, illustrated in Figure 4.2. When crystallization takes place at 120°C more peaks are observed and the most intense peaks are at slightly higher angles.

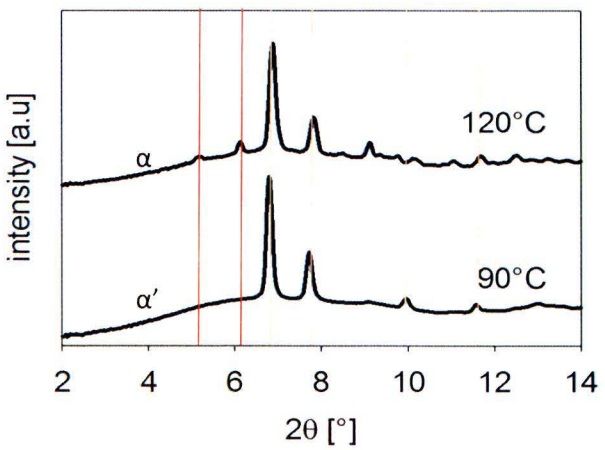

Figure 4.2 WAXD of isothermal crystallization from the melt at 120°C and 90°C

The effect of cooling rate is investigated in DSC by cooling from 240°C to 0°C at various rates. Figure 4.3a shows that the crystallization time, and so the crystallization temperature, is dependent on cooling rate. When the crystallization temperature is represented as a function of the crystallization time, a continuous cooling transformation (CCT) plot is obtained (see Figure 4.3b).

Figure 4.3 shows that, at a cooling rate of 10°C/min, no crystallization peak is observed, confirming the validity of the analysis with the TTT-time.

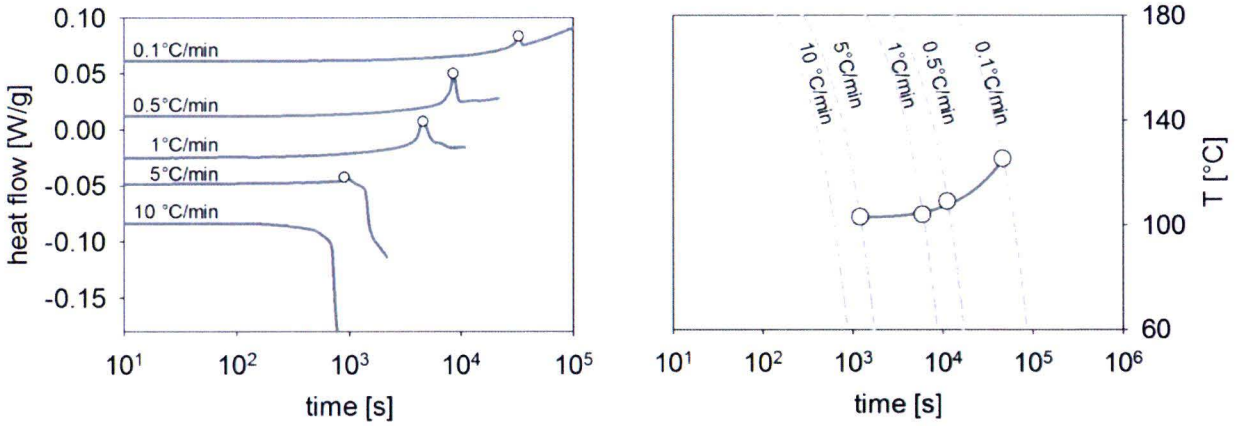

Figure 4.3 (a) Cooling thermograms at various cooling rates; (b) CCT-plot

During common production methods, cooling rates are high ($\dot{T} >> \dot{T}_{cr}$) and PLLA will be quenched amorphous. Therefore, samples for compression tests of next paragraph, are made by annealing quenched PLLA.

Similar to melt crystallization, annealing above T_g results in the α-form at high temperature and in the α'-form at low temperature. This is confirmed by WAXD (Figure 4.4): annealing at 90°C results in the α'-form, annealing at 120°C in the α-form.

The samples of the next paragraph are annealed for 7 hours at 80°C, resulting in the α'-form with a 24.7% WAXD crystallinity.

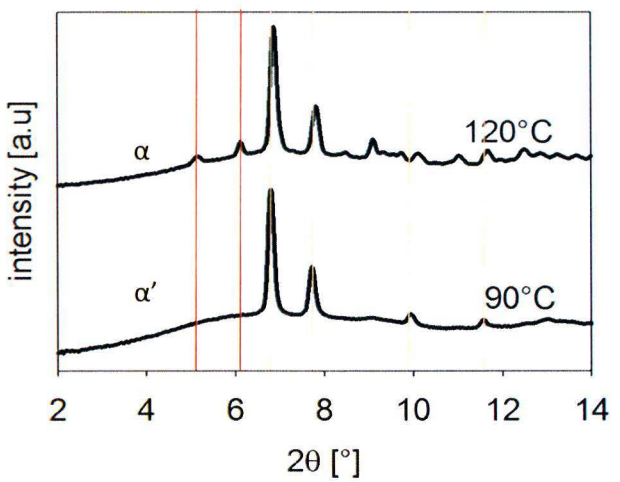

Figure 4.4 WAXD of isothermal crystallization from the solid at 120°C and 90°C

4.2 *Influence on mechanical properties*

To investigate the influence of crystallinity on the mechanical properties of PLLA, uniaxial compression tests at constant strain rate were performed on semi-crystalline sample, annealed as described before. Crystallinity restricts the molecular motion and this results in an increase of yield stress and in a decrease of yield drop. In Figure 4.5, which shows the influence of different annealing times on the stress-strain response, the yield drop decreases from 53 to 29 MPa.

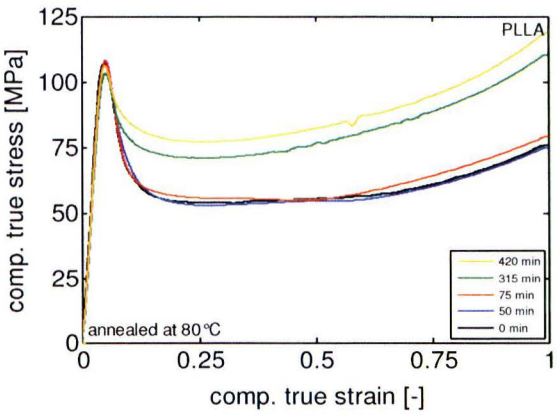

Figure 4.5 Influence of annealing time on stress strain curve

To highlight the influence of crystallization on the α- and β-processes of PLLA, the deformation kinetics are characterized by compression tests at different temperatures. Figure 4.6 shows the compression curves at 20°C and 50°C.

At 50°C, the yield stress decreased drastically with respect to the compression tests at 20°C, due to the temperature enhanced mobility. Further on, a larger decrease of yield drop with decreasing strain rate is observed at higher temperature. Compression tests at 50°C show that at low strain rates the yield drop becomes zero.

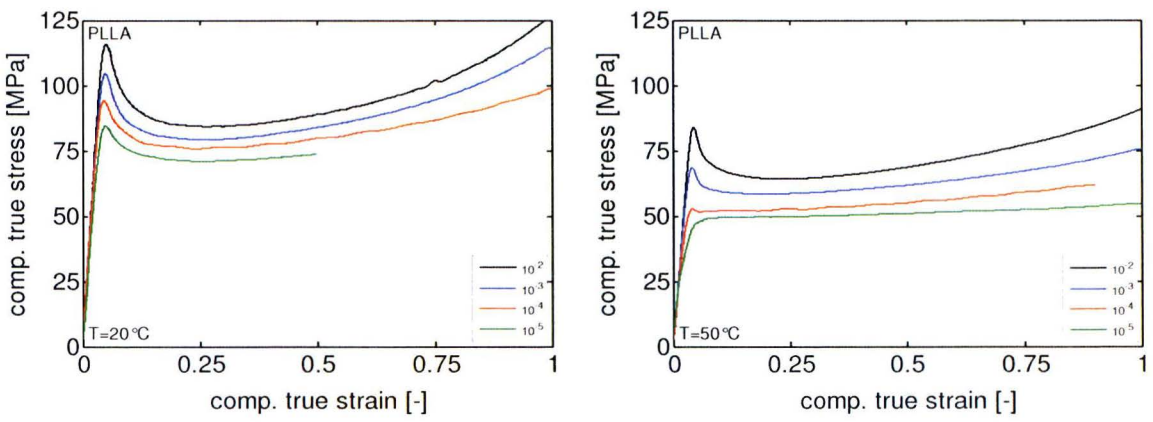

Figure 4.6 Compressions curves of semi-crystalline PLLA (a) at 20°C; (b) at 50°C

This phenomenon becomes more evident by plotting the strain rate dependence of the yield stress and lower yield, see Figure 4.7. The lower yield, corresponding to the α-process, has a linear relation with respect to the logarithmic strain rate. At 20°C, the yield stress also shows a linear relation with respect to the logarithmic strain rate. But, at 50°C at strain rates lower than 10^{-4} s^{-1}, no yield drop is observed, indicating that only the α-process is contributing to the deformation process.

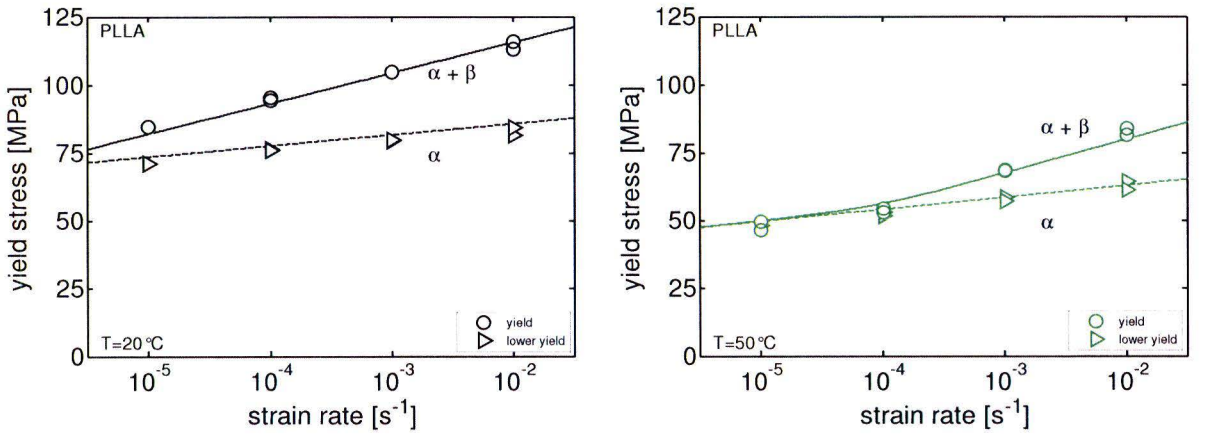

Figure 4.7 Strain rate dependence of the yield stress at 20°C and 50°C

An overview of data at various temperatures is given in Figure 4.8. Figure 4.8a illustrates the temperature dependent change of slope in the strain rate dependence of the yield drop and the decrease of yield stress by increasing temperature. Figure 4.8b illustrates decreasing lower yield at increasing temperature. Further on, it illustrates the linear dependence of the lower yield to the strain rate, independent of temperature.

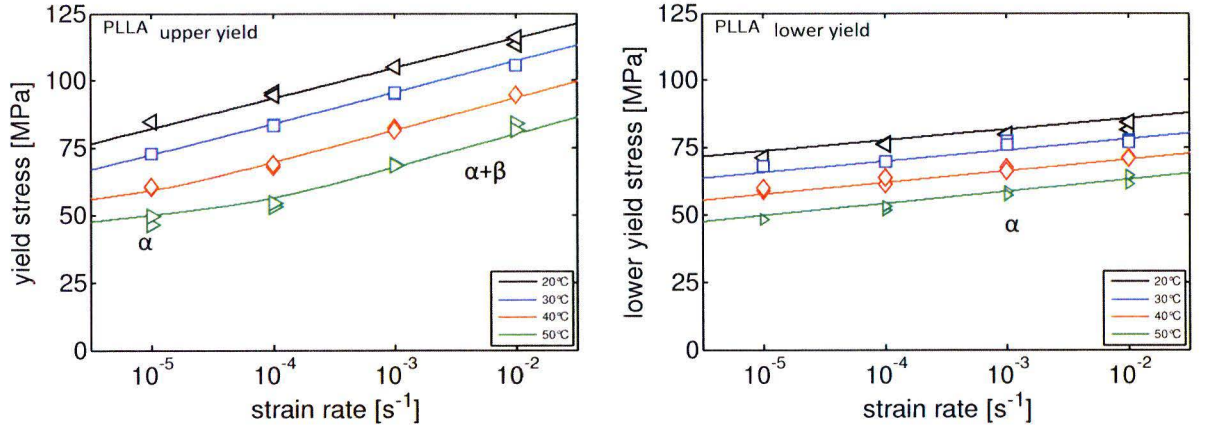

Figure 4.8 semi-crystalline PLLA at different temperatures: Rate dependence of (a) yield stress ; (b) lower yield stress

The fits of Figure 4.8 provided parameters (listed in table 4.1) to predict the time-to-failure with data of creep experiments. The resulting prediction is shown in Figure 4.9. Because the slope of the stress

dependence of time-to-failure is the same in negative value as the strain rate dependence of the yield stress, the same change in slope is observed.

At higher temperatures the slope decreases and time-to-failure becomes more dependent on stress which is beneficial for durability.

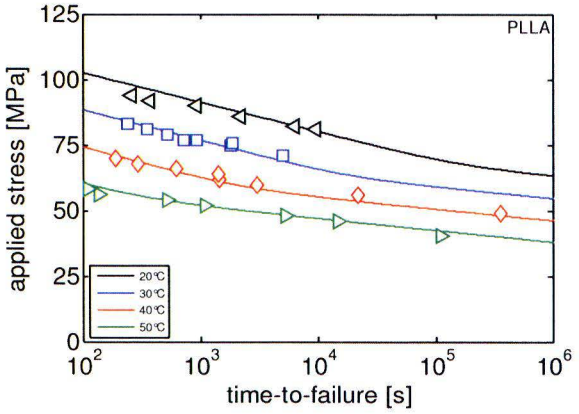

Figure 4.9 Semi-crystalline PLLA at different temperatures: Stress dependence of the time-to-failure

x	V_x^* [nm^3]	ΔU_x [kJ mol^{-1}]	$\dot{\varepsilon}_{0,x}^*$ [s^{-1}]	ε_{cr} [%]
α	2.3	425	$8 \cdot 10^{52}$	2.51
β	1.3	165	$7 \cdot 10^{22}$	2.51

Table 4.1 Ree-Eyring parameters

The increased strain rate dependence of the yield stress and the stress dependence of the time-to-failure of semi-crystalline PLLA, compared with amorphous PLLA, is illustrated in Figure 4.10.

Beside the shift of the β-process, the yield stresses and so the time-to-failure of semi-crystalline PLLA are increased due to reduced mobility, see Figure 4.10.

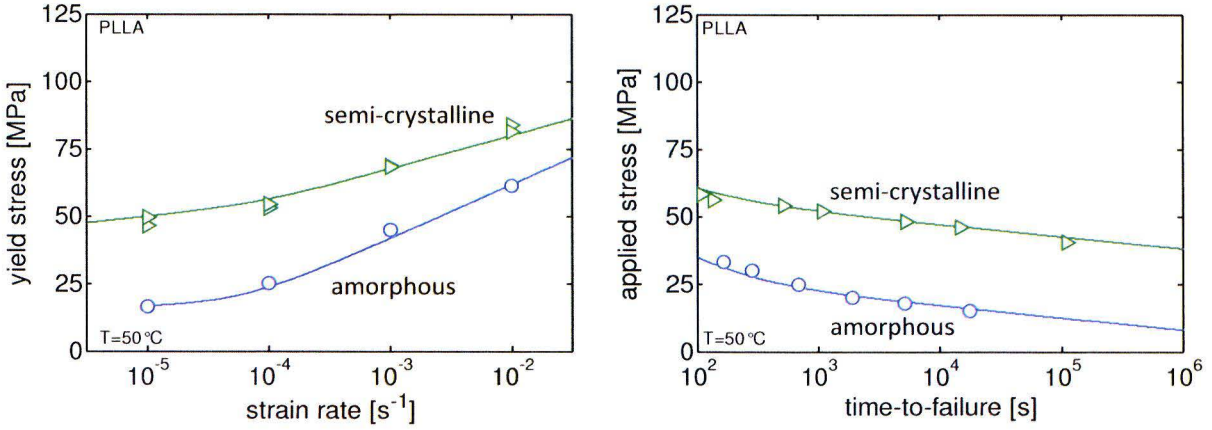

Figure 4.10 Semi-crystalline vs. amorphous PLLA at 50°C: (a) Rate dependence of the yield stress (b) Stress dependence of the time-to-failure

Already with 24.7% WAXD crystallinity, lifetime extends many decades. With an applied stress of 33 MPa, amorphous PLLA fails in less than 170 seconds. Whereas semi-crystalline PLLA fails only after few months.

Symmetrically, for an application that requires a lifetime of 10^4 seconds at 50°C, the maximum allowed stress for amorphous PLLA is 17 MPa, whereas for semi-crystalline PLLA it is 47 MPa.

Figure 4.10 demonstrates that crystallinity is beneficial for long term properties.

5 Part II: Enhancing crystallization of PLLA

As showed in the previous paragraph, crystallinity is beneficial for the life time of PLLA. Unfortunately, during common production methods like injection moulding, the cooling rates are too high ($\dot{T} >> \dot{T}_{cr}$) and PLLA is quenched amorphous. Crystallization by annealing at $T>T_g$ is not always desired, because products may deform and the process costs energy.

A way to enhance the crystallization on cooling is the formation of stereo complexes (SC). These structures are the result of the co-crystallization between PLLA and PDLA.

L-lactic acid D-lactic acid

Figure 5.1 (a) L-lactic acid; (b) D-lactic acid [13]

Pure PLLA or PDLA will only form homo-crystals (HC). In presence of the other enantiomer, hetero-crystals, containing L- and D-molecules, can also be formed.

Ikada et al. [14] first reported that the 1/1 association of PLLA and PDLA molecules can produce a stereo complex, a rare case of co-crystallization by simple lateral packing of molecule. The T_m of the stereo complex is around 230°C, i.e. about 50°C higher than T_m of the homo-crystals. Stereo complexes, acting like nucleating agents, can promote the growth of PLLA homo-crystals.

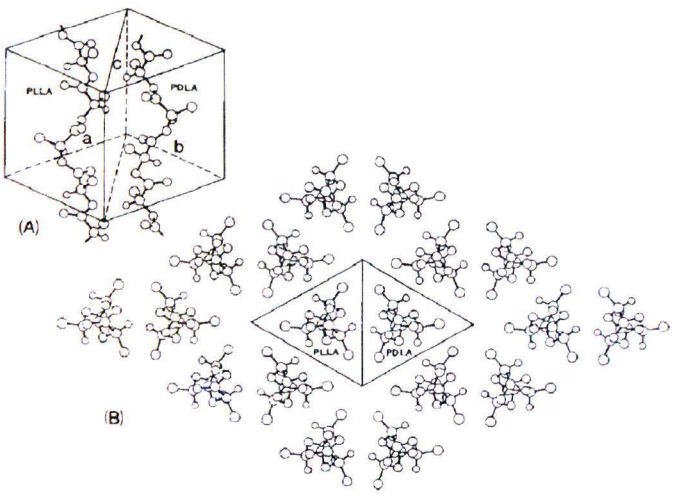

Figure 5.2 Crystal structure PLA stereo complex [13]

In this study to obtain stereo complexes, PLLA is blended with PDLA as described in paragraph 2.2.2. The crystallization behaviour is investigated with DSC. After melting at 240°C for two minutes, heat release is measured during cooling at 10°C/min, see Figure 5.3. While pure PLLA and PDLA do not crystallize at this cooling rate, the blends show crystallization peaks over the whole composition range. The efficiency in the formation of stereo complexes is dependent on molecular weight of PDLA, which is confirmed by the thermograms of Figure 5.3. Blends of PLLA and PDLA_HMw show two crystallization peaks, indicating the presence of both stereo complexes and homo-crystals. Blends of PLLA and PDLA_LMw show one crystallization peak in the composition range between 30% and 90%. In this range, all molecules associate in stereo complexes and no material crystallizes at low temperatures.

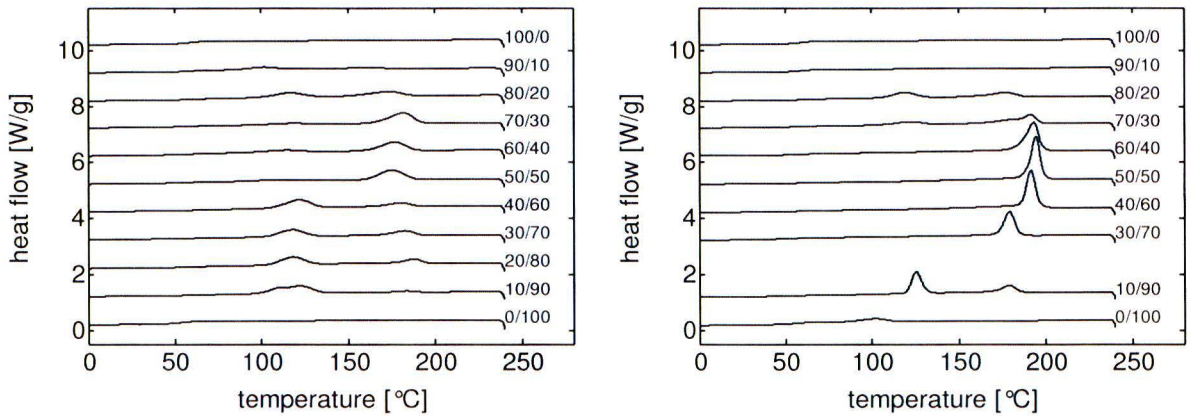

Figure 5.3 DSC thermogram on cooling at 10°C/min of (a) PLLA_PDLA_HMw_y/z; (b) PLLA_PDLA_LMw_y/z

The formation of only stereo complexes during cooling of the blend of PLLA_PDLA_LMw_60/40 is confirmed by WAXD (Figure 5.4). Cooling from 240°C at 10°C/min, shows a crystallization peak around 200°C. At lower temperatures, no other crystallization peaks appear, indicating that no other crystals are formed.

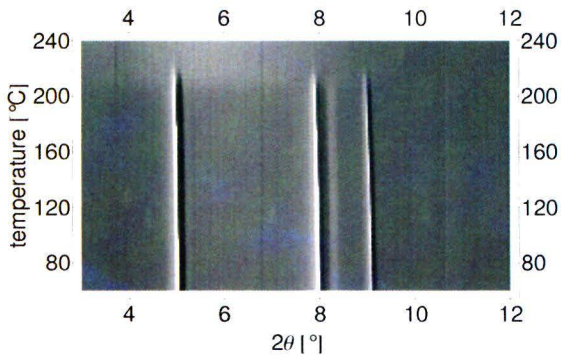

Figure 5.4 WAXD during cooling (10°C/min) of PLLA_PDLA_LMw_60/40

An overview of the crystallization behaviour is given by the phase diagrams of Figure 5.5, constructed by plotting crystallization temperatures (associated to peak maximum) versus composition. The phase diagrams for blends of PLLA with PDLA of different M_w exhibit similar features.

At high temperatures, PLLA and PDLA make a homogeneous solution. At intermediate temperature, PLLA and PDLA co-crystallize, forming stereo complexes. For certain blends , at low temperature, the leftover molecules crystallize as well.

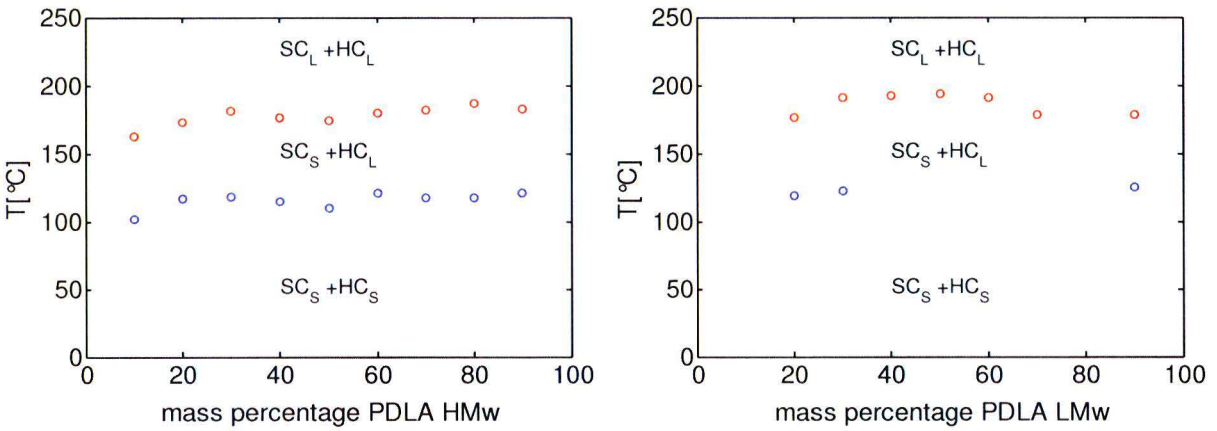

Figure 5.5 Phase diagrams on cooling at 10°C/min (a) Blends with PDLA_HMw; (b) Blends with PDLA_LMw [SC= stereo complex; HC= home-crystal]

Heat release resulting from the experiments of Figure 5.3 is represented in Figure 5.6.

The crystallinity can be obtained by dividing the amount of released heat by the latent heat of crystallization of 100% crystalline material, ΔH [J/g]. In literature, different values are given for PLLA and stereo complex, varying from respectively 93-203 J/g and 142-146 J/g [13]. Because it is not obvious which data is correct, no crystallinity is determined for data of Figure 5.6.

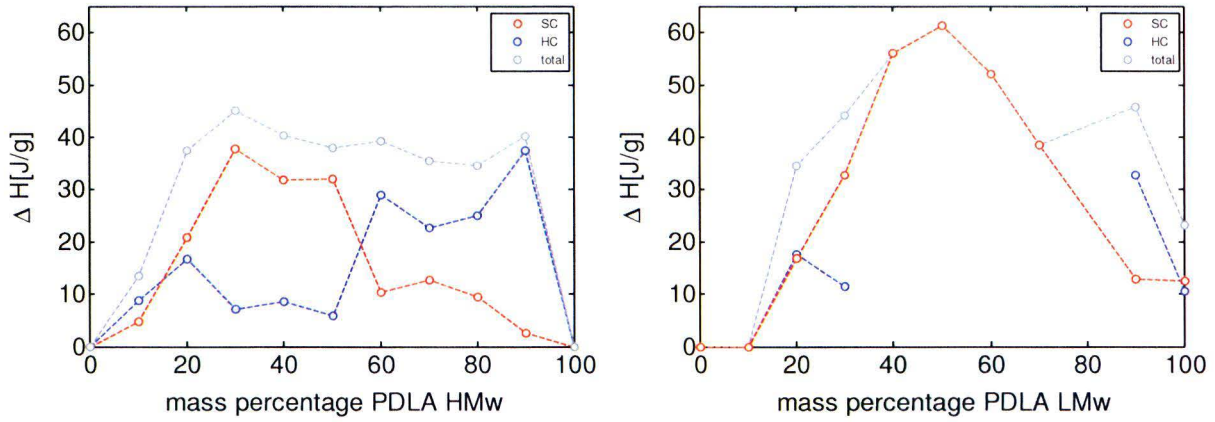

Figure 5.6 Heat release on cooling at 10°C/min (a) PLLA_PDLA_HMw_y/z; (b) PLLA_PDLA_LMw_y/z
[SC= stereo complex; HC= home-crystal]

Figure 5.6a shows the increase of total crystallization until 30% PDLA_HMw. From 60% on, the amount of stereo complex decreases and more homo-crystals are formed.

Figure 5.6b illustrates that blending with PDLA_LMw results in higher amount of crystallinity. The formation of stereo complex is larger, indicating blending with PDLA_LMw results in more effective crystallization.

5.1 Effect of coolingrate on stereo complex-formation

PLLA_PDLA_LMw_60/40 was selected to study the cooling rate dependence of stereo complex formation. Samples, compression moulded in films of 200 µm thickness, were cooled at very different rates, with different cooling methods. The structure was studied by WAXD. Results are given in Figure 5.7:

- Samples cooled in air ($\dot{T} \sim 1°C/sec$) shows 32.5% crystallinity.
- Samples cooled in cold plates ($\dot{T} \sim 10°C/sec$) shows 31% crystallinity
- Samples cooled in water ($\dot{T} \sim 100°C/sec$) shows no cyrstallinity

This means that the formation of stereo complexes can be suppressed at high cooling rates, in the range of 100°C/s, indicating that PDLA_LMw is not very effective as a nucleating agent.

Crystallinity versus cooling rate $\dot{T}$ is shown in Figure 5.7b. It can be seen that the amount of crystallinity decreases drastically with increasing $\dot{T}$.

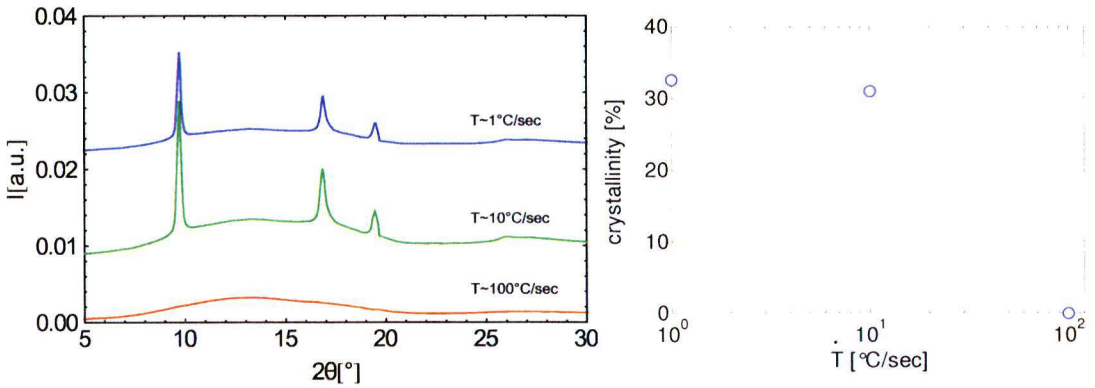

Figure 5.7 PLLA_PDLA_LMw_60/40: (a) WAXD of different cooling rates; (b) crystallinity vs. $\dot{T}$

5.2 *Influence of stereo complexes on mechanical properties*

To investigate the influence of stereo complexes on mechanical properties, uniaxial compression tests are performed. Compression curves at 23°C of PLLA_PDLA_LMw_60/40 (Figure 5.8) show that the yield drop vanishes: only the α-process is contributing to the deformation.

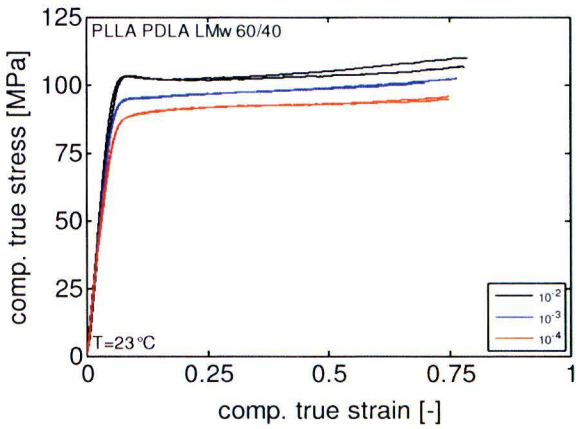

Figure 5.8 Stress vs. true strain of PLLA_PDLA_LMw_60/40

The resulting strain rate dependence of the yield stress is illustrated in Figure 5.9a, which compares PLLA and PLLA_PDLA_LMw_60/40. Due to the absence of the β-process, the slope of PLLA_PDLA_LMw_60/40 is lower and constant over the whole range of strain rate.

The decreased mobility of the molecules results in an increase of the yield stress with respect to amorphous PLLA. The strain rate dependence decreased from 14 to 6.4 MPa per decade.

This decrease of slope makes the lifetime more dependent on stress (see Figure 5.9b) and is therefore beneficial for the durability of the material

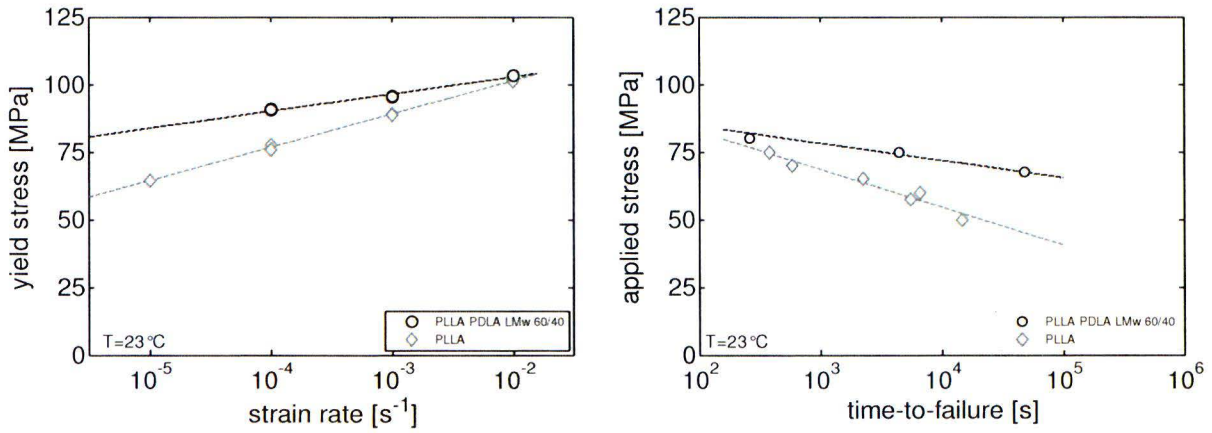

Figure 5.9 PLLA vs. PLLA_PDLA_LMw_60/40 at 23°C (a) Rate dependence of yield stress; (b) Stress dependence of time-to-failure

Besides the increased life time, the absence of strain hardening makes PLLA_PDLA_LMw_60/40 still a brittle material. The brittle behaviour is confirmed by tensile testing: PLLA_PDLA_LMw_60/40 breaks brittle at a maximum strain of 1.8%, before yielding (see Figure 5.10a). Figure 5.10b illustrates the short life-time of PLLA_PDLA_LMw_60/40 in tension.

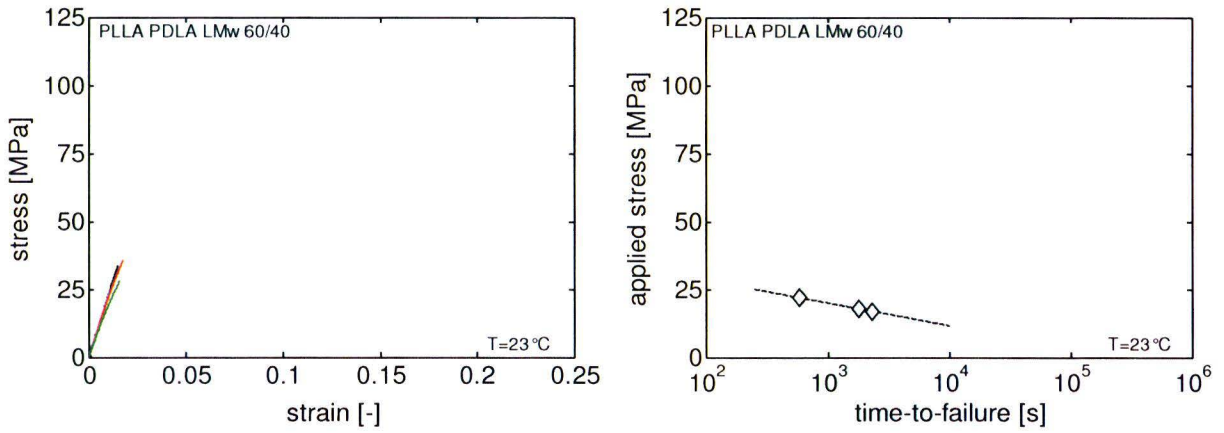

Figure 5.10 PLLA_PDLA_LMw_60/40 in tension: (a) Tensile curves; (b) Stress dependence of the time-to-failure

Figure 5.11 Brittle failed sample

6 Part III: Toughness of PLLA

6.1 *Influence of water absorbtion*

When PLLA is used in the human body, the influence of water absorption on the mechanical properties become important, since water acts as a plasticizer. Observations on PLDLLA spinal cages showed that the effect of wetting is similar to that of increase in temperature [15].

To investigate the influence of water absorption, tensile test are done in water at 37°C.

Preparatory to the tests, tensile bars were stored in water at 37°C for several weeks to absorb water (see Figure 6.1).

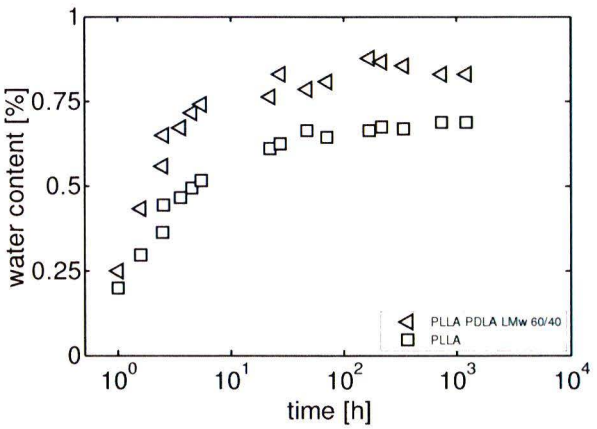

Figure 6.1 Water absorption

Figure 6.2 shows the tensile curves in respectively the dry and wet environment. A decrease of yield stress is observed, e.g. at a strain rate of 10^{-3} s^{-1} the yield stress decreases from 52 MPa to 39 MPa. This decrease, due to enhanced mobility, is also illustrated in Figure 6.3a.

Figure 6.3b illustrates the effect of water absorption on the lifetime of PLLA. As was seen for yield stress, also the time-to-failure decreases for a certain applied stress.

Further on, brittle failure is observed for all wetted samples, whereas dry samples show a neck at low strain rates. This suggests degradation in water.

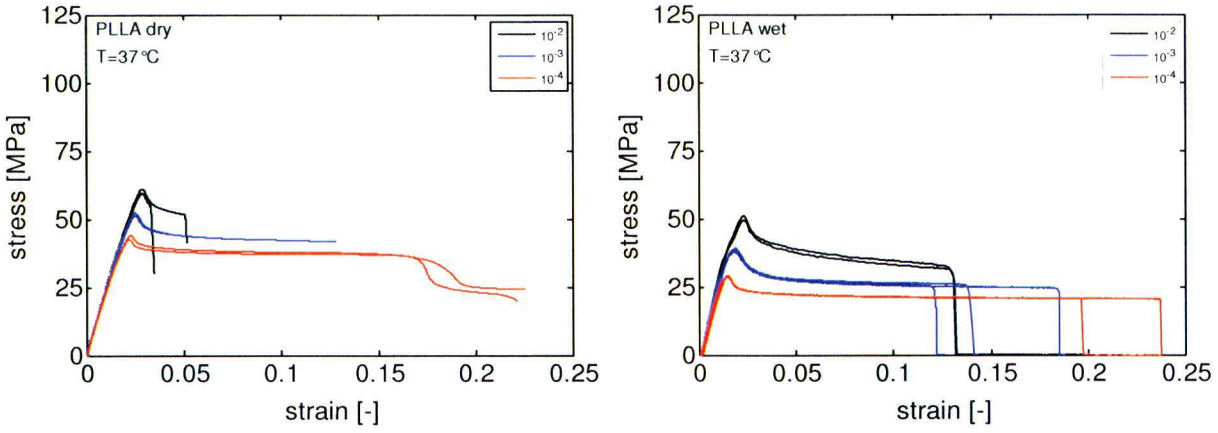

Figure 6.2 Tensile curves of PLLA at 37°C (a) dry; (b) in water

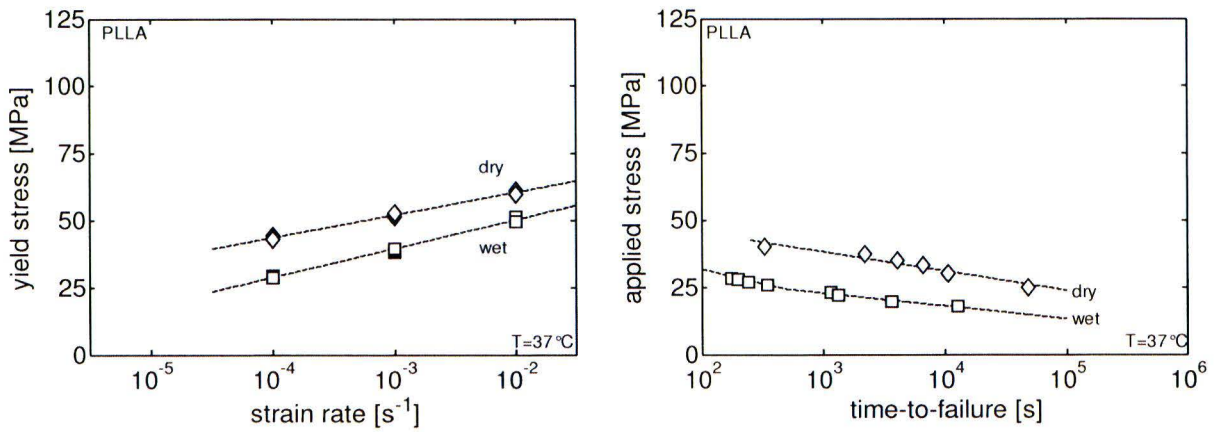

Figure 6.3 Comparison dry vs. wet PLLA (a) Strain rate dependence of yield stress; (b) Stress dependence of time-to-failure

6.2 *Influence of adding core-shell nano particles*

A possible route to improve toughness PLLA, is the addition of core-shell nano particles.

PLLA and PLLA_PDLA_LMw_60/40 are blended with 15% EXL, as described in paragraph 2.2.2.

Figure 6.4a illustrates the deformation behaviour in tension of PLLA and PLLA+15EXL. Due to the added core-shell nano particles, the yield stress decreases 23MPa and the strain at failure increases tremendously. This indicates that the toughness of PLLA is improved, confirmed by the mode of failure: PLLA shows crazing and fails brittle, PLLA+15EXL necks.

The decreasing effect of the core-shell nano particles on the time-to-failure is illustrated in Figure 6.4b. For a certain applied stress, the lifetime decreases one and a half order of magnitude.

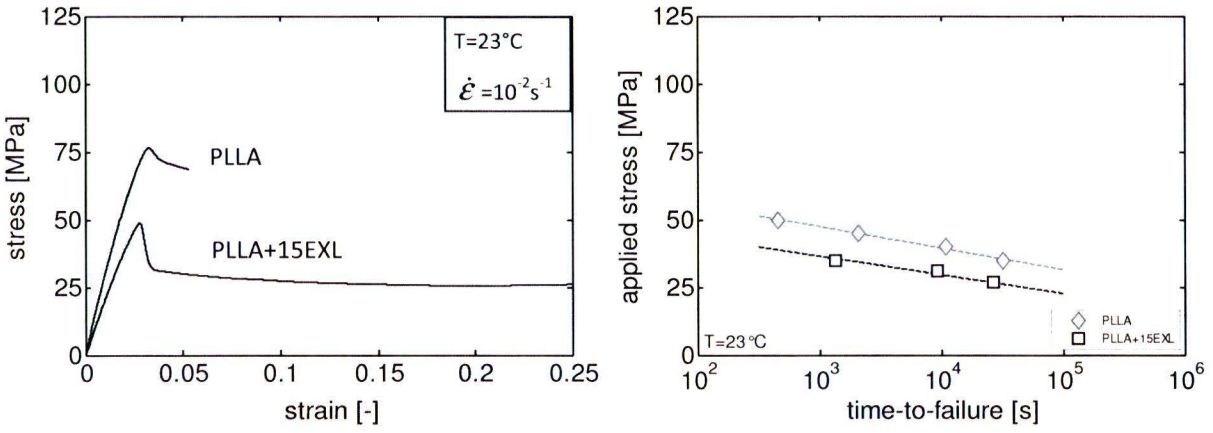

Figure 6.4 Tensile curves at 23°C of (a) PLLA; (b) PLLA+15EXL

The effect of toughening of PLLA_PDLA_LMw_60/40 is shown in Figure 6.5.

In tension, stress at failure increases from 34 to 45 MPa. Strain at failure increases from 0.015 to 0.024, see Figure 6.5a.

Where adding core-shell nano particles led to decreased time-to-failure for PLLA, for PLLA_PDLA_LMw_60/40 it results in a slight increase of time-to-failure. Compared to time-to-failure in compression, time-to-failure in tension is tremendously short, see Figure 6.5b.

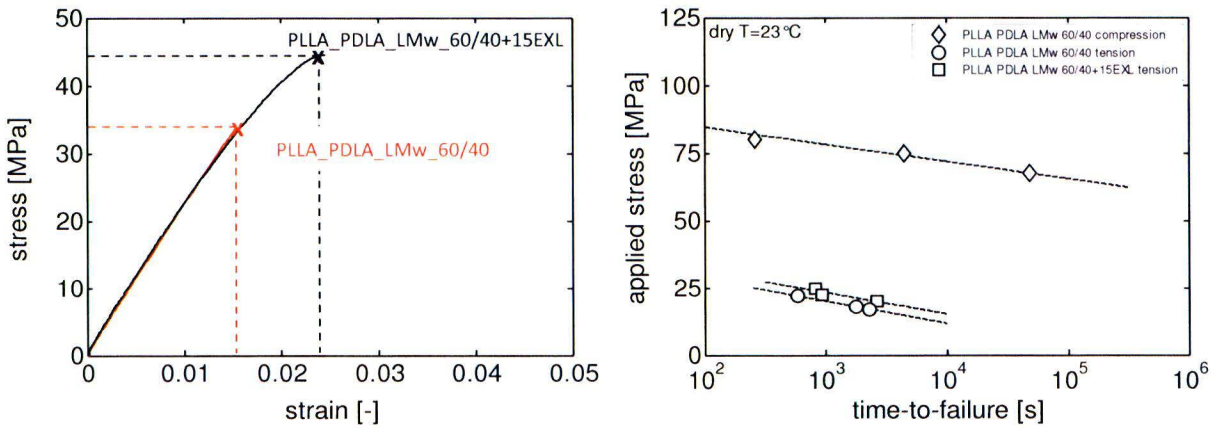

Figure 6.5 (a) Tensile curves of PLLA_PDLA_LMw_60/40+15EXL; (b) Stress dependence of time-to-failure, influence of added EXL

7 Conclusions

- The time-to-failure of PLLA in static loading conditions can be increased drastically by crystallization
- The time-scales required for crystallization of pure PLLA is too long to obtain reasonable crystallization during common processing methods
- The time-scale can be substantially improved by blending with PDLA to form stereo complexes, acting as nucleating agents
- Obtained time-scales are still too long for processing
- A possible solution is the use of heated moulds
- To improve toughness, PLLA can be blended with core shell particles

8 Bibliography

[1] M. R. Krijnen, M. G. Mullender, T. H. Smit, V. Everts, and P. I. J. M. Wuisman, "Radiographic, Histologic, and Chemical Evaluation of Bioresorbable 70/30 Poly-L-lactide-CO-D, L-lactide Interbody Fusion Cages in a Goat Model," *Spine*, vol. 31, no. 14, 2006.

[2] A. Schindler and D. Harper, "Polylactide. II. ViscosityΓÇômolecular weight relationships and unperturbed chain dimensions," *Journal of Polymer Science: Polymer Chemistry Edition*, vol. 17, no. 8, pp. 2593-2599, 1979.

[3] H. Tsuji, S. H. Hyon, and Y. Ikada, "Stereocomplex formation between enantiomeric poly(lactic acid)s. 4. Differential scanning calorimetric studies on precipitates from mixed solutions of poly(D-lactic acid) and poly(L-lactic acid)," *Macromolecules*, vol. 24, no. 20, pp. 5657-5662, Sept. 1991.

[4] T. Engels, S. Sontjens, T. Smit, and L. Govaert, "Time-dependent failure of amorphous polylactides in static loading conditions," *Journal of Materials Science: Materials in Medicine*, vol. 21, no. 1, pp. 89-97, Jan. 2010.

[5] O. D. Sherby and J. E. Dorn, "Anelastic creep of polymethyl methacrylate," *Journal of the Mechanics and Physics of Solids*, vol. 6, no. 2, pp. 145-162, 1958.

[6] C. Bauwens-Crowet, J.-M. Ots, and J.-C. Bauwens, "The strain-rate and temperature dependence of yield of polycarbonate in tension, tensile creep and impact tests," *Journal of Materials Science*, vol. 9, no. 7, pp. 1197-1201, July 1974.

[7] L. van Breemen. Contact mechanics in glassy polymers PhD Thesis. pag. 33-55.

[8] H. Eyring, "Viscosity, Plasticity, and Diffusion as Examples of Absolute Reaction Rates," *The Journal of Chemical Physics*, vol. 4, no. 4, pp. 283-291, Apr. 1936.

[9] T. Ree and H. Eyring, "Theory of non-Newtonian flow. I. Solid plastic system," *Journal of Applied Physics*, vol. 26, no. 7, pp. 793-800, 1955.

[10] R.P.M.Janssen. Quantitative Prediction of Polymer Failure PhD. Thesis. pag. 76. 2007.

[11] T. Miyata and T. Masuko, "Crystallization behaviour of poly(l-lactide)," *Polymer*, vol. 39, no. 22, pp. 5515-5521, Oct. 1998.

[12] T. Kawai, N. Rahman, G. Matsuba, K. Nishida, T. Kanaya, M. Nakano, H. Okamoto, J. Kawada, A. Usuki, N. Honma, K. Nakajima, and M. Matsuda, "Crystallization and Melting Behavior of Poly (l-lactic Acid)," *Macromolecules*, vol. 40, no. 26, pp. 9463-9469, Nov. 2007.

[13] H. Tsuji, "Poly(lactide) Stereocomplexes: Formation, Structure, Properties, Degradation, and Applications," *Macromolecular Bioscience*, vol. 5, no. 7, pp. 569-597, 2005.

[14] Y. Ikada, K. Jamshidi, H. Tsuji, and S. H. Hyon, "Stereocomplex formation between enantiomeric poly(lactides)," *Macromolecules*, vol. 20, no. 4, pp. 904-906, Apr. 1987.

[15] T. H. Smit, T. A. P. Engels, P. I. J. M. Wuisman, and L. E. Govaert, "Time-Dependent Mechanical Strength of 70/30 Poly(l,dl-lactide): Shedding Light on the Premature Failure of Degradable Spinal Cages," *Spine*, vol. 33, no. 1, 2008.